Karttunen, Anssi; von Hertzen, Raimo

Dynamic response of a cylinder cover under a moving load

Published in:
International Journal of Mechanical Sciences

DOI:
10.1016/j.ijmecsci.2014.03.026

Published: 01/01/2014

Document Version
Peer-reviewed accepted author manuscript, also known as Final accepted manuscript or Post-print

Please cite the original version:
Karttunen, A., & von Hertzen, R. (2014). Dynamic response of a cylinder cover under a moving load. *International Journal of Mechanical Sciences*, *82*, 170-178. https://doi.org/10.1016/j.ijmecsci.2014.03.026

Dynamic response of a cylinder cover under a moving load

Anssi T. Karttunen[a,*], Raimo von Hertzen[a]

[a]*Department of Applied Mechanics, Aalto University, Finland*

Abstract

Cylinders with thin covers are used in high-speed rolling contact industrial applications such as a two-cylinder soft calender of a paper machine. In this paper, the dynamic behavior of an elastic cylinder cover is studied using a 1D Pasternak-type foundation model with Kelvin-Voigt damping. The cover is subjected to a moving point load, which is taken to represent a load resultant due to rolling contact. Analytical expressions for the natural frequencies, vibration response, wave dispersion relation, total strain energy and dissipation power of the cover are obtained. To validate the 1D approach, the calculated natural frequencies and modes are compared to those given by a 2D plane strain finite element model, and a good agreement is found. The critical load speed at which traveling waves first appear in the cover is derived for the undamped analytical model on the basis of a resonance condition. The critical speed is shown to be also the minimum phase velocity of the waves in the cover. When damping is included, the wave speeds decrease, lowering also slightly the critical speed, which, in addition, becomes blurred due to the damping. Once a traveling wave has emerged, it remains in the cover also at supercritical speeds due to a spectrum of resonant speeds induced by wave dispersion. At supercritical speeds, reinforced resonances are observed when the head and tail of a traveling wave interact. High shear damping leads to a substantial increase in dissipation power related to heat generation and rolling resistance of the cover already at subcritical speeds.

Keywords: Pasternak foundation, moving load, critical speed, traveling wave, reinforced resonance, power dissipation

1. Introduction

Along with the advances in materials science, the development of cylinder cover materials for rolling contact industrial machines, for example soft calenders of paper machines, has taken major steps forward in recent years. The replacement of the traditional metal-to-metal contact by novel polymers and composites in high-speed rolling contact applications has proven to be beneficial in terms of end product quality and modifiability. However, the covers induce and suffer from detrimental dynamic phenomena which have not been fully explained yet, let alone dealt with. Examples of these phenomena are the self-excited vibration mechanism, barring, which is caused by viscoelastic cover deformations acting as time-delayed feedbacks in a rolling contact system [1, 2], and a contact-induced traveling wave phenomenon occurring at high rolling speeds, which is the subject of this study.

The study of cylinder cover dynamics constitutes essentially a 2D plane strain problem where typically a relatively long hard cylinder with a thin soft cover is rolling in contact with another cylinder. It is crucial to note that the plane strain feature establishes a fundamental distinction between covered cylinders and, for example vehicle tires and flexible train wheels, which are often studied by using ring or shell models. In other words, the traveling waves in cylinder covers should not be viewed too closely in terms of other circular structures.

Recompiled, unedited accepted manuscript. **Cite as**: *Int. J. Mech. Sci.* 2014;82:170-178. doi link

*Corresponding author. *anssi.karttunen@iki.fi*

Only a few studies addressing traveling waves in thin cylinder covers can be found. In a recent paper, Qiu developed a 2D semianalytical plane strain model for a covered cylinder rolling in contact with a rigid surface [3]. He calculated the natural frequency spectrum for the covered cylinder and used the frequencies to estimate the critical rolling speed at which traveling waves start to emerge in a cover. To understand the nature of the traveling wave phenomenon to a deeper extent, we recently utilized a 2D plane strain finite element (FE) model to study a polymer-covered cylinder rolling in contact with a steel cylinder [4]. We found that at the critical speed of the covered cylinder, the minimum speed of Rayleigh waves in the cover is actually reached and both primary and secondary Rayleigh waves arise at the leading edge of the contact area. The superposition of the waves leads to the formation of a strong traveling wave in the cover. The phenomenon may be considered as a Rayleigh wave resonance [5]. A similar wave propagation phenomenon is encountered, for example, when a high-speed train approaches the Rayleigh wave speed of the train-track subsoil, see, for example, [6].

The detailed account on the physical characteristics of the traveling wave phenomenon in a thin cylinder cover under rolling contact [4] acts as a basis for the current study. The central novel feature of this paper is that we show how the dynamic 2D plane strain cover problem can be essentially reduced to 1D. The development of such a reduced model is motivated by the general notion that a 1D model should be more convenient to work with both analytically and computationally than a 2D model.

In more detail, we study traveling waves in a cylinder cover subjected to a moving constant radial point load using a 1D Pasternak-type foundation model with Kelvin-Voigt damping. The cover vibration is investigated using a modal expansion technique and the wave propagation offers a complementary perspective via wave dispersion analysis. The natural frequencies and modes calculated from the 1D analytical model are compared to those given by a 2D plane strain FE model to show that the 1D model captures the essential features of the 2D problem. A major outcome from the 1D approach is that it allows the effortless calculation of the relevant resonant load speeds, dispersion curves and vibration response unlike semianalytical [3] or purely numerical methods [4, 7–10]. The transient cover response sheds light on the emergence of traveling waves in the cover. The calculated steady-state response demonstrates the effect of cover damping in a detailed manner, showing how the retardation of the response with respect to the the moving load is explained by sub- and supercritical modes; how the traveling waves emerge in the cover for different values of cover damping; and how the damping affects the power dissipation of the cylinder cover at sub- and supercritical speeds.

2. Theory and physical interpretation

2.1. Equation of motion and vibration response

The system under investigation is depicted schematically in Fig. 1. The 1D model consists of a non-rotating rigid cylinder with a cover subjected to a moving radial point load P. In other words, an actual case of rolling contact is studied as an inverted problem [11]. The effect of the rotation of the cylinder will be discussed later, but it will turn out that it is not of crucial importance for the current study. In reality, the load would be a distributed one, but since the contact area, the nip, is typically relatively small in rolling contact machines, it is reasonable to present the load resultant as a point force acting at the load center. The cover is modeled as a Pasternak-type foundation consisting of a shear layer attached to a Kelvin-Voigt assembly.

When the traveling wave phenomenon takes place under rolling contact in a 2D system, the dominant modes of vibration are those of the primary mode family (see Fig. 20 in [4]). Furthermore, at such an instance, the displacement path of a point near the cover surface due to a traveling wave (Rayleigh wave) is strongly elliptic with the radial displacements clearly dominating over the tangential ones. On the basis of the foregoing, a single-mode approximation is used for the radial deformation u of the shear layer in the 1D model to capture the primary mode family, but the tangential deformations are not taken into account. It will be shown in Section 3.1 that this is a good approximation of the primary mode family of a 2D model.

The model in Fig. 1 is quite similar to the one by Chatterjee et al. [12]. Their treatment, however, was largely different from ours. They used their model to study waves in rotating tires by formulating a

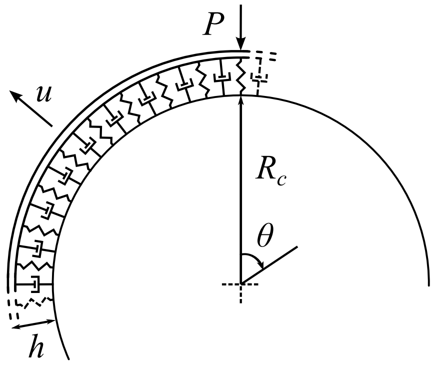

Figure 1: 1D Analytical model for a covered cylinder subjected to circumferentially moving point load P. The cover is modeled as a shear layer attached to a Kelvin-Voigt base, and u is the radial displacement of the shear layer.

non-linear boundary value contact problem associated with steady-state rolling conditions. We employ a circumferentially moving point load catching the essentials of the traveling wave phenomenon in the cylinder cover. In the following, the complete vibration response is derived for the system of Fig. 1.

The equation of motion in a coordinate system fixed to the cylinder in terms of the radial displacement u of the shear layer reads

$$u_{tt} + \frac{E}{\rho h^2} u + \frac{\alpha}{\rho h^2} u_t - \frac{\kappa G}{\rho R^2} u_{\theta\theta} - \frac{\kappa \beta}{\rho R^2} u_{\theta\theta t} = P(\theta, t) \; . \tag{1}$$

Above, E is the Young's modulus and G is the shear modulus of the cover, and α and β are the corresponding strain rate damping parameters, respectively. The density and thickness of the cover are ρ and h, respectively. The radius $R = R_c + h/2$ is used to determine the effective width of a material element. In addition, we introduce a shape factor κ for the shear layer, which accounts for the total shear force on the cover layer cross-section similarly to the shear coefficient of a Timoshenko beam. Thus, in principle, the shape factor introduces a 2D effect to the model. The value of the shape factor is determined computationally in Section 3.1 with the aid of a 2D plane strain FE model. For a moving constant point load, we have $P(\theta, t) = P_0 \delta(\theta - \Omega t)$, where P_0 is the load amplitude and Ω is the angular velocity of the load. The rotational frequency of the load is $f_{\text{rot}} = \Omega/2\pi$. The model description is completed by the requirement of continuity of the displacement and slope which leads to

$$u(0, t) = u(2\pi, t) \quad \text{and} \quad u_\theta(0, t) = u_\theta(2\pi, t) \; . \tag{2}$$

Note that the term containing $u_{\theta\theta}$ in Eq. (1) stems from the Pasternak foundation model and is typical for all shear layer models. This term couples the adjacent material elements to each other. For a derivation of the Pasternak foundation model, see [13], by the aid of which the dynamic equation of motion Eq. (1) can be easily derived by taking into account the mass of the cover lumped to the shear layer.

Each natural mode, $\sin(n\theta)$ or $\cos(n\theta)$, of the free undamped cover consists of n full waves on the cover circumference, with the exception of $n = 0$, which is the breathing mode. As n increases, the wavelength in a mode decreases. The solution for the moving load problem can be expanded in terms of the natural modes leading to

$$u(\theta, t) = \sum_{n=1}^{\infty} \left[c_n(t) \sin(n\theta) + d_n(t) \cos(n\theta) \right] + d_0(t) \; . \tag{3}$$

By substituting Eq. (3) into Eq. (1), the modal expansion coefficients c_n, d_n and d_0 can be calculated from the equations

$$\ddot{c}_n + 2\zeta_n \omega_n \dot{c}_n + \omega_n^2 c_n = \frac{P_0}{\pi} \sin(n\Omega t) \; , \tag{4}$$

$$\ddot{d}_n + 2\zeta_n\omega_n\dot{d}_n + \omega_n^2 d_n = \frac{P_0}{\pi}\cos(n\Omega t) \ , \tag{5}$$

$$\ddot{d}_0 + 2\zeta_0\omega_0\dot{d}_0 + \omega_0^2 d_0 = \frac{P_0}{2\pi} \ , \tag{6}$$

where the natural angular frequencies and modal damping ratios are given by $(n = 0, 1, 2, \ldots)$

$$\omega_n = \sqrt{\frac{1}{\rho}\left(\frac{E}{h^2} + \frac{\kappa G}{R^2}n^2\right)} \ , \tag{7}$$

$$\zeta_n = \frac{\alpha/h^2 + \kappa\beta n^2/R^2}{2\rho\omega_n} \ , \tag{8}$$

respectively. With zero initial conditions, $u(\theta, 0) = 0$ and $u_t(\theta, 0) = 0$, all the initial conditions for the modal equations also become zero. Thus, when the system is initially at rest, the complete vibration response can be shown to be

$$\begin{aligned} u(\theta,t) &= \sum_{n=1}^{\infty} A_n \cos\left[n(\Omega t - \theta) - \phi_n\right] + \frac{P_0}{2\pi\omega_0^2} \\ &- \sum_{n=1}^{\infty} A_n \mathrm{e}^{-\zeta_n\omega_n t}\left\{\frac{1}{\sqrt{1-\zeta_n^2}}\left[\zeta_n\cos(n\theta+\phi_n) + \frac{n\Omega}{\omega_n}\sin(n\theta+\phi_n)\right]\sin\omega_{\mathrm{dn}}t + \cos(n\theta+\phi_n)\cos\omega_{\mathrm{dn}}t\right\} \\ &- \frac{P_0}{2\pi\omega_0^2}\mathrm{e}^{-\zeta_0\omega_0 t}\left(\frac{\zeta_0}{\sqrt{1-\zeta_0^2}}\sin\omega_{\mathrm{d0}}t + \cos\omega_{\mathrm{d0}}t\right) \ , \end{aligned} \tag{9}$$

where the top row represents the steady-state response and the rows below provide the transient response. The amplitudes A_n and the phase shifts ϕ_n are calculated from the expressions

$$A_n = \frac{P_0}{\pi\sqrt{\left[\omega_n^2 - (n\Omega)^2\right]^2 + (2\zeta_n\omega_n n\Omega)^2}} \ , \tag{10}$$

$$\tan\phi_n = \frac{2\zeta_n\omega_n n\Omega}{\omega_n^2 - (n\Omega)^2} \quad , \quad 0 \le \phi_n < \pi \quad (n = 1, 2, \ldots) \ , \tag{11}$$

and the damped natural angular frequencies ω_{dn} from

$$\omega_{\mathrm{dn}} = \omega_n\sqrt{1-\zeta_n^2} \qquad (n = 0, 1, 2, \ldots) \ . \tag{12}$$

The amplitude A_n reaches its peak value at $n\Omega = \omega_{\mathrm{pn}} = \omega_n\sqrt{1-2\zeta_n^2}$ $(\zeta_n < 1/\sqrt{2})$. The total strain energy of the cover in steady-state can be decomposed into compression and shear parts as

$$E_{\mathrm{tot}} = E_c + E_s = \frac{\pi R E l}{2h}\left(\sum_{n=1}^{\infty} A_n^2 + \frac{P_0^2}{2\pi^2\omega_0^4}\right) + \frac{\pi\kappa G h l}{2R}\sum_{n=1}^{\infty} n^2 A_n^2 \ , \tag{13}$$

where l is the length of the cylinder in axial direction. Analogously, the total dissipation power of the cover in steady-state becomes

$$P_{\mathrm{tot}} = P_c + P_s = \frac{\pi R\alpha l}{h}\Omega^2\sum_{n=1}^{\infty} n^2 A_n^2 + \frac{\pi\kappa\beta h l}{R}\Omega^2\sum_{n=1}^{\infty} n^4 A_n^2 \ . \tag{14}$$

2.2. Critical speed and wave propagation considerations

It can be seen from Eq. (10) that without damping the nth mode is in resonance when $\omega_n = n\Omega$. Therefore, the resonant angular velocity Ω_n of the load for each mode is given by

$$\Omega_n = \frac{\omega_n}{n} = \sqrt{\frac{1}{\rho}\left(\frac{E}{n^2h^2} + \frac{\kappa G}{R^2}\right)} \ , \tag{15}$$

which is of the same form ($\Omega_n = \omega_n/n$) as the one given by Soedel and Padovan [14–16] for the tire standing wave phenomenon, where traveling waves arise from the contact patch between road and vehicle tire. The lowest resonant speed is achieved in the limit $n \to \infty$, which leads to the critical angular speed of the system

$$\Omega_{\mathrm{cr}} = \sqrt{\frac{\kappa G}{\rho R^2}} \ . \tag{16}$$

In terms of tangential load velocity on the cover surface, the critical speed in the undamped case is

$$v_{\mathrm{cr}} = \hat{R}\sqrt{\frac{\kappa G}{\rho R^2}} \ , \tag{17}$$

where $\hat{R} = R_c + h$. It can be seen from Eq. (16) that the critical speed is independent of the Young's modulus of the cover. Note that the critical angular speed is an accumulation point of the angular velocities Ω_n for $n \to \infty$. Therefore, at the critical speed, a large number of natural modes are in resonance or very close to it simultaneously.

To further elucidate the dynamic behavior of the system, the dispersion relation for traveling waves in the shear layer is obtained from Eq. (1) by a solution of the form $u = \mathrm{e}^{\mathrm{i}(k\hat{R}\theta - \omega t)}$, which leads to

$$\omega(k) = \pm\sqrt{\frac{1}{\rho}\left(\frac{E}{h^2} + \frac{\kappa G}{R^2}\hat{R}^2k^2\right)} \ , \tag{18}$$

where $k = 2\pi/\lambda$ is the wavenumber. The phase velocity is defined as $v = \omega/k$. Thus, in the small wavelength limit $k \to \infty$, Eq. (18) yields for the minimum phase velocity the expression

$$v_{\min} = \hat{R}\sqrt{\frac{\kappa G}{\rho R^2}} \equiv v_{\mathrm{cr}} \ . \tag{19}$$

Therefore, the critical speed based on the resonance condition equals the minimum phase velocity of the waves in the shear layer. Similarly, for a 2D cover model the critical speed can be estimated in elastic and quasi-elastic cases according to the Rayleigh wave velocity, which is a certain portion of the shear wave velocity of an elastic half-space [4].

To form a standing wave vibration mode in the cover from two identical waves traveling in opposite directions, the wavenumber must satisfy $k = n/\hat{R}$, that is, the cylinder circumference must be divisible by the wavelength $\lambda_n = 2\pi\hat{R}/n$ of the wave. In this case, the discrete dispersion relation and wave propagation velocities of the traveling waves are given by

$$\omega(n) = \pm\sqrt{\frac{1}{\rho}\left(\frac{E}{h^2} + \frac{\kappa G}{R^2}n^2\right)} \ , \tag{20}$$

$$v(n) = \pm\hat{R}\sqrt{\frac{1}{\rho}\left(\frac{E}{n^2h^2} + \frac{\kappa G}{R^2}\right)} \quad \text{or}$$

$$\Omega(n) = \pm\sqrt{\frac{1}{\rho}\left(\frac{E}{n^2h^2} + \frac{\kappa G}{R^2}\right)} \ , \tag{21}$$

respectively. It can be seen that Eqs. (15) and (21) are equivalent, and Eq. (21) describes how the wave velocity increases due to wave dispersion at lower values of n. We can conclude that when a vibration resonance due to the moving point load takes place in the cylinder cover, from a different point of view, a traveling wave arises in the cylinder cover as a result of the superposition of waves, similarly to the Rayleigh wave resonance [4, 5].

By taking the damping of the cylinder cover into account, the discrete dispersion relation (Eq. (20)) becomes

$$\omega_d(n) \equiv \pm\omega(n)\sqrt{1-\zeta_n^2} = \pm\omega_{\mathrm{dn}} \ , \tag{22}$$

which shows that for high values of n the decrease in the wave frequencies becomes marked because of the high modal damping ratios ζ_n, see Eq. (8). Furthermore, the frequency decrease causes the waves propagating in the cover to slow down, which in turn might reduce the critical speed for the traveling wave phenomenon. However, as can be seen from Eq. (10), at the same time the modal amplitudes A_n are effectively made lower by the damping, especially for higher modes, as both n and ζ_n increase. Due to this, it is difficult to determine a certain critical speed at which the traveling waves due to the moving load can be first observed explicitly. Therefore, the critical speed in the damped case becomes blurred in contrast to the well-defined critical speed of the undamped case. Ultimately, this provides the motive to study the emergence of the traveling waves in the damped case by computational means in this paper.

2.3. The effect of rotation

Let us briefly study the case of a rotating cylinder. If the covered cylinder were to rotate with an angular velocity Ω, the centrifugal force acting on the cover due to rotation would be taken into account in Eq. (1) by adding the term $\Omega^2(R+u)$ on the RHS. The term $\Omega^2 R$ would superpose a constant displacement

$$u_0 = \frac{\Omega^2 R}{E/(\rho h^2) - \Omega^2} \tag{23}$$

to the general solution given by Eq. (9), which could be combined with the already existing constant $P_0/2\pi\omega_0^2$ in the solution. This would only change the compressional (or extensional) strain energy by a constant but would have no effect on the dissipated power or on the traveling wave phenomenon. Therefore, Eq. (23) has no essential significance to the solution.

The term $\Omega^2 u$ on the RHS could be combined with the term $E/(\rho h^2)u$ on the LHS of Eq. (1), leading to the term $[E/(\rho h^2) - \Omega^2]u$ on the LHS. It can be seen that all equations developed in Sections 2.1 and 2.2 would still be valid provided that the substitution $E/(\rho h^2) \to E/(\rho h^2) - \Omega^2$ was made. The undamped natural angular frequencies and modal damping ratios, in particular, would be given by

$$\omega_{n,\mathrm{cen}} = \sqrt{\frac{1}{\rho}\left(\frac{E}{h^2} + \frac{\kappa G}{R^2}n^2\right) - \Omega^2} \ , \tag{24}$$

$$\zeta_{n,\mathrm{cen}} = \frac{\alpha/h^2 + \kappa\beta n^2/R^2}{2\rho\omega_{n,\mathrm{cen}}} \ , \tag{25}$$

respectively. Note, however, that the relation $2\zeta_{n,\mathrm{cen}}\omega_{n,\mathrm{cen}} = 2\zeta_n\omega_n$ is valid. In this case, the resonant angular velocities would be calculated from

$$\Omega_{n,\mathrm{cen}} = \sqrt{\frac{n^2}{n^2+1}} \cdot \sqrt{\frac{1}{\rho}\left(\frac{E}{n^2h^2} + \frac{\kappa G}{R^2}\right)} \ . \tag{26}$$

It can be seen that the centrifugal force does not change the critical angular speed of the system, since still $\Omega_{n,\mathrm{cen}} \to \sqrt{\kappa G/(\rho R^2)}$, when $n \to \infty$. The centrifugal force, on the other hand, affects the resonant load angular velocities at low mode numbers n, that is, at very high speeds. The effect of the centrifugal force on the steady-state solution is accounted for by substituting the natural angular frequencies of Eq. (7) by

Table 1: Parameter values for the system of Fig. 1 adapted from an industrial test machine.

Young's modulus	$E = 18$ MPa
Shear modulus	$G = 6$ MPa
Compression damping parameter	$\alpha = 50$ Ns/m^2
Shear damping parameter	$\beta = 16.67$ Ns/m^2
Poisson ratio	$\nu = 0.5$
Density	$\rho = 2000$ kg/m^3
Cover thickness	$h = 0.01$ m
Cylinder radius	$R_c = 0.204$ m
Cylinder length	$l = 0.2$ m
Shape factor	$\kappa = 6/7$

those given by Eq. (24) in Eqs. (10) and (11). For the value $\nu = 0.5$ of the Poisson ratio of a polymeric cylinder cover, we have $E = 3G$, and it is easy to see that

$$\frac{\omega_{n,\mathrm{cen}}}{\omega_n} = \sqrt{1 - \frac{(\Omega/\Omega_{\mathrm{cr}})^2}{\frac{3R^2}{\kappa h^2} + n^2}} \ . \tag{27}$$

We can estimate that typically for covered cylinders $3R^2/\kappa h^2 \gtrsim 1000$. Then, for $\Omega \leq 3\Omega_{\mathrm{cr}}$, excluding extremely high rotational speeds, we get

$$1 \geq \frac{\omega_{n,\mathrm{cen}}}{\omega_n} \geq 0.995 \quad \text{for all}\, n \ . \tag{28}$$

Note also that near the critical speed the steady-state response is dominated by the resonating modes for which $n \geq 100$, leading to $1 \geq \omega_{n,\mathrm{cen}}/\omega_n \geq 0.9996$. It can be concluded that for rotational speeds accessible to real machines the centrifugal force has a negligible effect on the system response and, thus, the inverted approach with a load moving on a non-rotating cylinder is suitable for the study of the traveling wave phenomenon. This is also demonstrated by example calculations for the material parameters used in this work in Figs. 3(b) and 8(a).

3. Computational results and discussion

3.1. Comparison between 1D and 2D cover models and the dynamic properties of the 1D model

The parameters used in the calculations are listed in Table 1. With the damping parameter value $\alpha = 50$ Ns/m^2, the damping ratio attains the value of 1 for the mode $n = 2968$, that is, $\zeta_{2968} = 1$. In this paper, we use the modes $n = 0, 1, 2, \ldots, 1000$ in the computations. In Fig. 2(a), the undamped natural frequencies $f_n = \omega_n/2\pi$ of the 1D analytical model calculated from Eq. (7) for two different cover thicknesses are compared to those given by a 2D plane strain FE model similar to the one utilized in [4]. The same parameter values are used for both models, apart from the shape factor κ present only in the analytical model and obtained by adjusting the analytical 1D results to those calculated from the 2D FE model. With the shape factor $\kappa = 6/7$, we find a good agreement between the two different models, especially at higher natural modes. Interestingly, the same shape factor is obtained from the widely-used Cowper's formula $\kappa = 10(1 + \nu)/(12 + 11\nu)$ for a rectangular cross-section Timoshenko beam with the Poisson ratio $\nu = 0.5$ [17].

Fig. 2(b) presents the normalized radial displacements for the modes $n = 35$ and $n = 100$ in the case of both the 1D analytical model and the 2D FE model. For the 1D model the displacements are given by $\sin(n\theta)$ and for the 2D model the displacements are those calculated at the cover surface. For $n = 100$, the calculated natural frequencies for the 1D and 2D models are 4146 and 4147 Hz, respectively. The

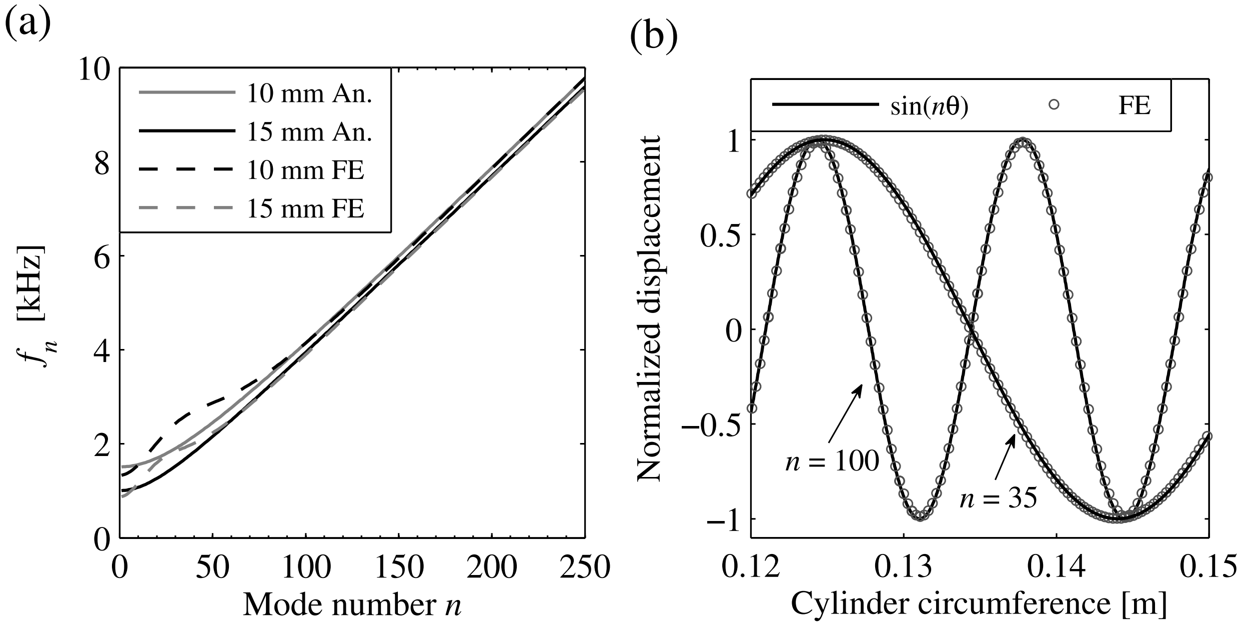

Figure 2: (a) Undamped natural frequencies of both the 1D analytical cover model (solid lines) and the 2D FE model (dashed lines) for cover thicknesses of 10 and 15 mm. The results are in good concordance, especially at the higher modes. (b) Normalized radial displacements for the modes $n = 35$ and $n = 100$ along the cylinder cover circumference for the cover thickness 10 mm. For the 1D analytical model the displacements are given by $\sin(n\theta)$ and the displacements of the 2D FE model are those calculated at the cover surface.

correspondence between the models is good and the mode shapes coincide also at higher and lower modes. The differences in the natural frequencies between the two models at the lower modes in Fig. 2(a) are due to the distinctive throughout-thickness behavior of the two cover models. The difference is biggest for $n = 35$, for which the calculated natural frequencies are 2001 and 2558 Hz for the 1D and 2D models, respectively. The 2D model captures the dispersive wave characteristics of the cylinder cover in a more detailed manner, especially in the case of lower modes, since these modes penetrate deeper into the cover and interact with the bottom of the cover layer. However, the higher modes are of primary interest in the study of the traveling waves, mainly due to the fact that they appear at lower load speeds and indicate the speed range of the system within which the traveling waves first start to appear. We conclude that the 1D model captures the essential features of the 2D cylinder cover problem.

To see, which modes resonate at a given rotational frequency of the load, we consider the resonance condition (15) divided by 2π in the form $f_{\mathrm{rot},n} = f_n/n$. Fig. 3(a) shows the resonant rotational frequencies f_n/n and f_{dn}/n in the undamped and damped cases, respectively. In addition, the corresponding curve f_{pn}/n for the modal amplitude peak response is presented. In the undamped case, the critical rotational frequency of the load under which no modes are in resonance is 38.65 Hz. In terms of the tangential load velocity, the undamped critical speed is 52 m/s, which equals the minimum phase velocity of the traveling waves in the cover and is practically the same as the Rayleigh wave speed in an elastic half-space for the current material parameters [18]. It can be seen that in the damped case the resonances start to take place at rotational frequencies lower than 38.65 Hz and one may ask whether traveling waves should also start to arise in the cover below the undamped critical speed. Note, however, that the higher natural modes, and traveling waves associated with them, are damped effectively so that it is impossible to determine from Fig. 3(a) a certain critical speed at which the behavior characteristic to the traveling wave phenomenon could be first detected. Similar conclusions can be drawn from the modal amplitude peak curve. The onset of the traveling wave phenomenon in the presence of damping will be discussed in the next section.

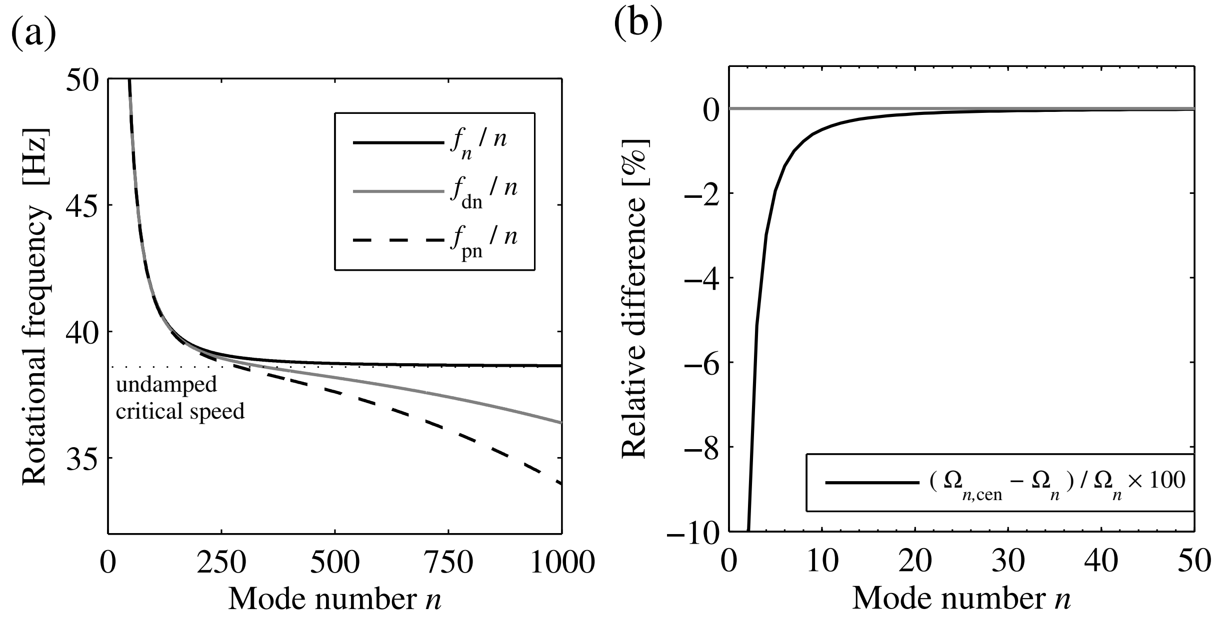

Figure 3: (a) Resonant rotational frequencies for the undamped, damped and peak amplitude cases f_n/n, f_{dn}/n and f_{pn}/n as a function of the resonating mode number n, respectively. (b) Effect of the centrifugal force on the resonant load angular velocities. The centrifugal force decreases the resonant speeds of the lowest modes.

The effect of the centrifugal force on the resonant speeds is studied in Fig. 3(b). The figure shows the relative difference between the resonant angular velocities calculated from Eqs. (15) and (26). It can be seen that the centrifugal force is significant only for the lowest modes ($n < 10$) corresponding to very high load velocities, which are of secondary interest in the study of the emergence of the traveling waves.

Fig. 4 presents the steady-state modal phase shifts ϕ_n ($n = 1, 2, \ldots$) calculated from Eq. (11) as a function of the rotational frequency of the moving load. The parameters given in Table 1 are used. The effect of damping can be clearly seen in the figure. For lower modes, the modal damping is small and the phase shift of 180 degrees in the vicinity of resonance occurs quickly, whereas for higher modes the change is not that steep. The small damping of lower modes causes the resonance modal amplitudes to be notably larger, in general, for the lower modes. It should be noted, however, that a large number of higher modes are in resonance nearly simultaneously when the traveling waves start to arise slightly below 40 Hz in contrast to high load speeds with only one lower mode being clearly dominant at a time.

3.2. Vibration response of the cylinder cover

In Fig. 5, the complete vibration response of the cover calculated from Eq. (9) is presented in a case in which the rotational frequency of the load is 46.09 Hz, which has been chosen according to the resonant speed of mode $n = 60$. The load is applied at $t = 0$ s for zero displacement and velocity initial conditions. As the load moves, a traveling wave front can be seen to form. The first wave in the front grows quickly to its full extent and others soon follow. At the point of entry ($\theta = 180^o$), the cover is left to vibrate freely in a harmonic manner radiating waves to both directions. As the transient phase fades out, only the traveling steady-state wave front remains in the cover. The wave front which is almost in steady-state is well-depicted between $t = 8 - 10$ ms and $\theta = 270 - 340^o$.

Fig. 6 shows the steady-state response of the cover at three different rotational frequencies of the moving point load P. In Fig. 6(a) the response is clearly quasi-static in the sense that there are no traveling waves present. The displacements are practically symmetric with respect to the loading point. In Fig. 6(b), at the rotational frequency of 40 Hz, an incipient traveling wave can be seen on the trailing edge of the load.

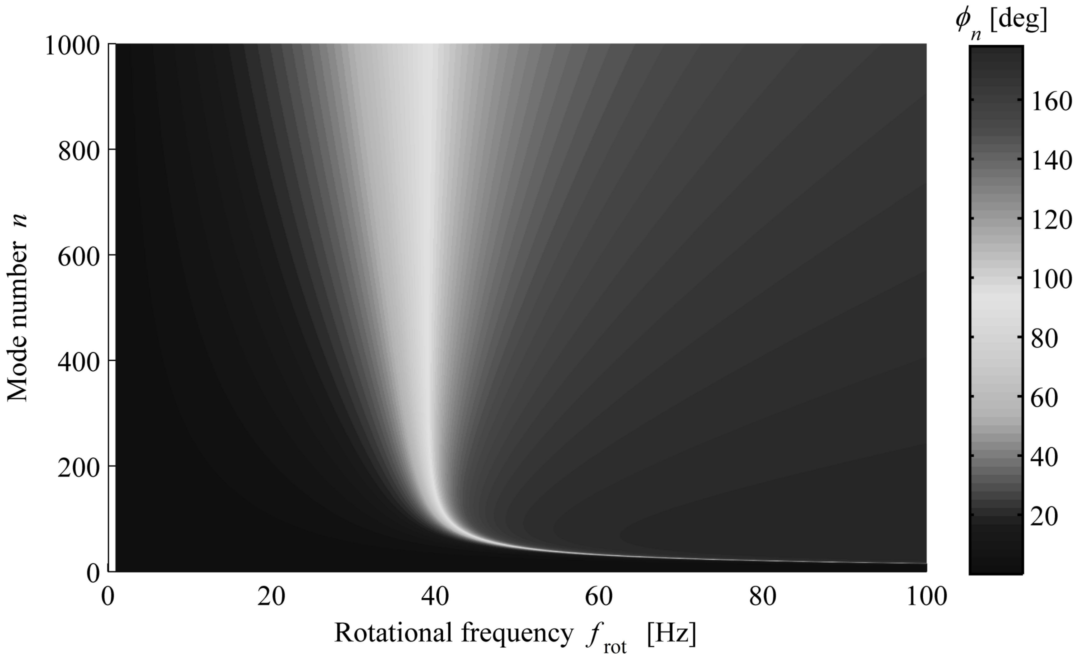

Figure 4: Steady-state modal phase shifts of the cylinder cover natural modes. The bright white curve corresponds to the phase shift value of 90^o, and it divides the plane into subcritical and supercritical excitation regimes. In the area of higher modes, this curve becomes almost vertical at the undamped critical rotational frequency 38.65 Hz. Strong damping causes the resonance phase change to occur in a milder fashion for the higher modes.

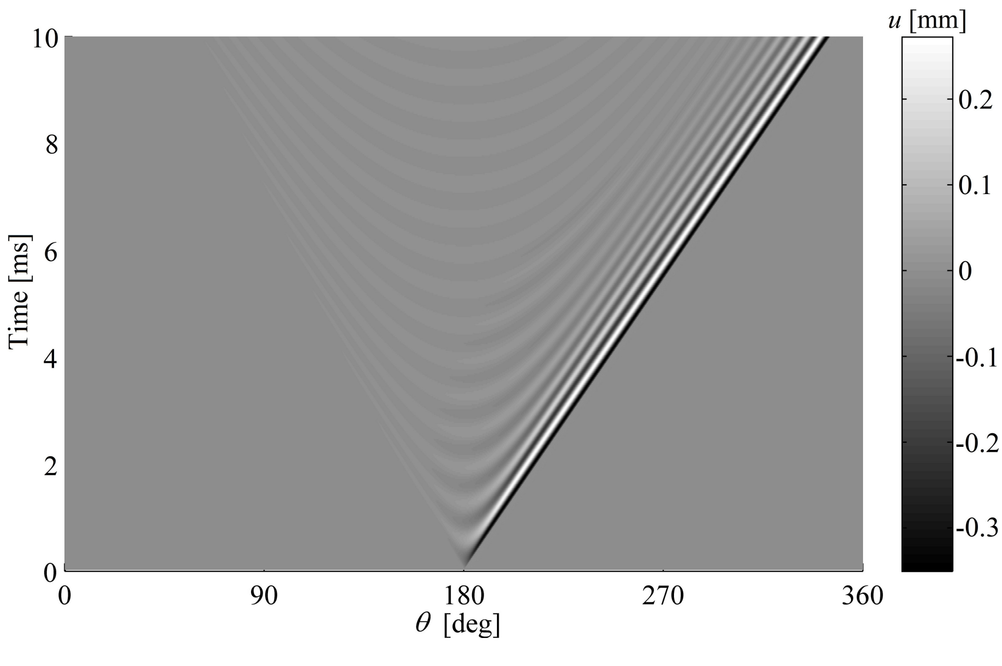

Figure 5: Complete vibration response of the cylinder cover. The moving point load with the rotational frequency 46.09 Hz is applied at $t = 0$ s at $\theta = 180^o$. A horizontal cut gives a momentarily picture of the waves around the cylinder circumference. The curved patterns are related to the transient response.

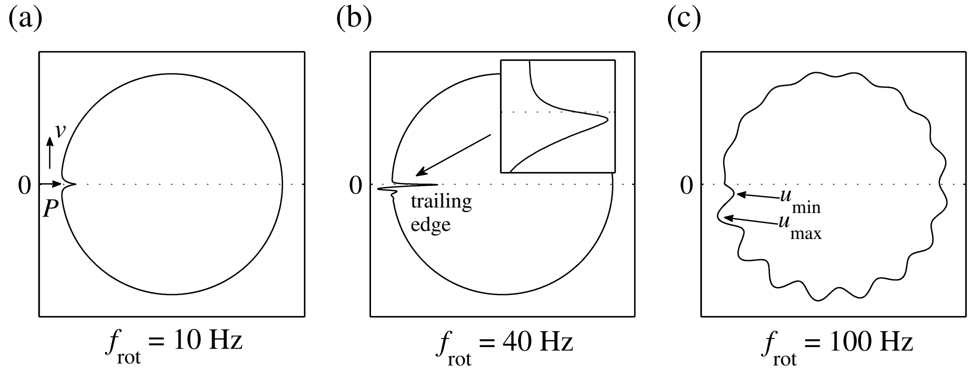

Figure 6: Deformed shape (i.e., the radial displacements) of the cylinder cover at three different rotational frequencies of the load. (a) 10 Hz, a quasi-static case; (b) 40 Hz, an incipient traveling wave on the trailing edge and (c) 100 Hz, strong traveling wave around the whole cylinder circumference. The dotted line indicates the location of the point load.

Near the loading point, the radial displacement minimum has more than tripled in comparison to Fig. 6(a). The load has also started to "climb up the hill" from the displacement minimum in the same manner as in the case of an elastic ring [19]. By the aid of the current model, the climbing is explained by the fact that for the supercritically excited modes, the cover response lags the excitation due to the post-resonance phase shift, while subcritically excited modes are still nearly in the same phase with the excitation. The climbing is more evident in Fig. 6(c), in which a strong traveling wave is present at a higher speed. Note that the steady-state response (see Eq. (9)) is symmetric with respect to the location $\theta = \Omega t$ if the phase shifts ϕ_n are all zero. Therefore, since at low rotational frequencies $\phi_n \approx 0$, the response is practically symmetric. When the rotational frequency increases, the phase shifts start to grow from zero (see Fig. 4), which destroys the symmetry of the response and, finally, leads to the generation of the traveling wave. In Fig. 6(c), the locations of the minimum and maximum radial displacements are pointed out; they are always located in the same manner behind the load when a traveling wave is present.

In Fig. 7, the steady-state response of the cylinder cover for the rotational frequency range 1–100 Hz of the moving load is shown. The response can be seen to be rather quasi-static up till 40 Hz, after which a traveling wave forms. Near 60 Hz, the wave goes around the whole cylinder circumference. It can be also seen that when the rotational frequency increases, so does the wavelength of the traveling wave. The determination of an exact critical speed in the damped case may be difficult, since the wave emerges gradually. Thus, pointing out a narrow critical speed range, in which the waving clearly starts to occur, may be more sensible. Similarly, Padovan concluded that there does not exist a single so-called critical speed when damping is included into a tire model, but there is a range of speeds over which the tire standing wave phenomenon appears to develop [16].

Fig. 8 displays the minimum and maximum wave displacements within the cover circumference in the rotational frequency range 1–100 Hz for three different values of the damping parameter α ($\beta = \alpha/3$). With the low damping parameter value $\alpha = 5$ Ns/m^2, the peaks of $u_{\min}$ and $u_{\max}$ occur at the rotational frequencies of 39.2 and 40 Hz, respectively. With even smaller damping, the peaks come closer to each other. With higher damping, the peaks of $u_{\min}$ and $u_{\max}$ take place at higher rotational frequencies. With $\alpha = 100$ Ns/m^2, for example, the peak of $u_{\max}$ occurs at $f_{\text{rot}} = 48.5$ Hz. At rotational frequencies above the peaks, the displacements for high damping start to settle down to more moderate values.

With low damping, $u_{\max}$ and $u_{\min}$ can be clearly seen to exhibit local maximums and minimums at supercritical rotational frequencies at which a traveling wave extends over the cylinder's circumference. At rotational frequencies, at which $u_{\max}$ and $u_{\min}$ attain local maximums and minimums, respectively, the displacement response of the traveling wave is dominated by a resonating mode. Note that the mode resonances become more distinct at higher speeds. If the mode number of the resonating mode is n, the traveling wave appears as if it was a decaying harmonic wave containing an integer number of full waves

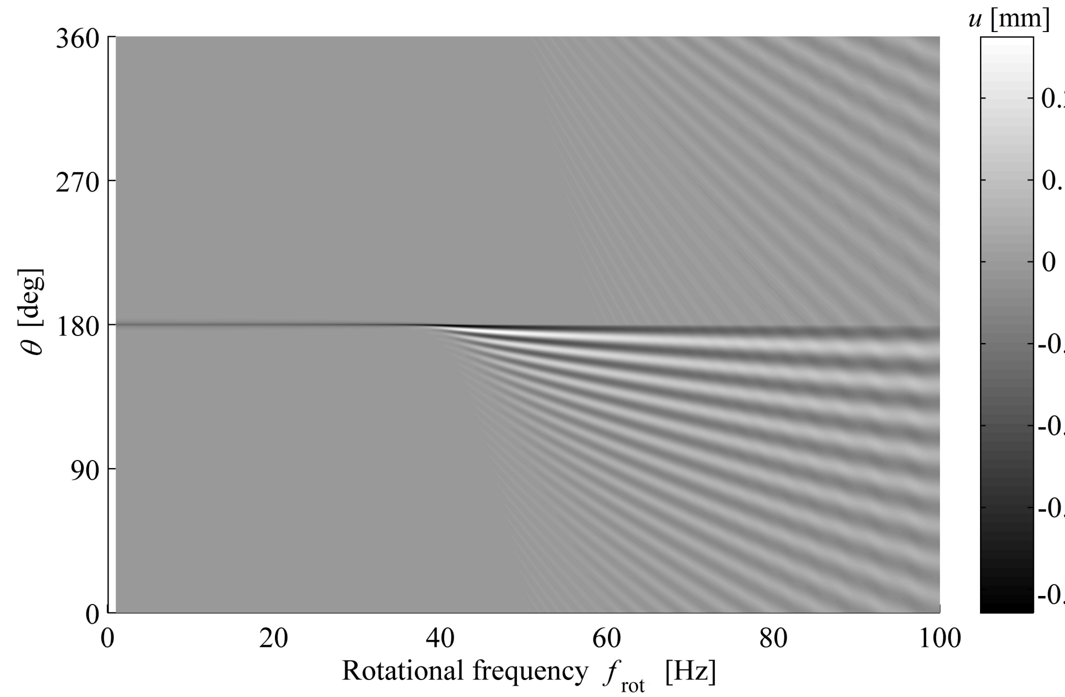

Figure 7: Steady-state response of the cylinder cover for the rotational frequency range 1–100 Hz of the moving point load. A vertical cut gives the steady-state response picture of the waves around the cylinder circumference.

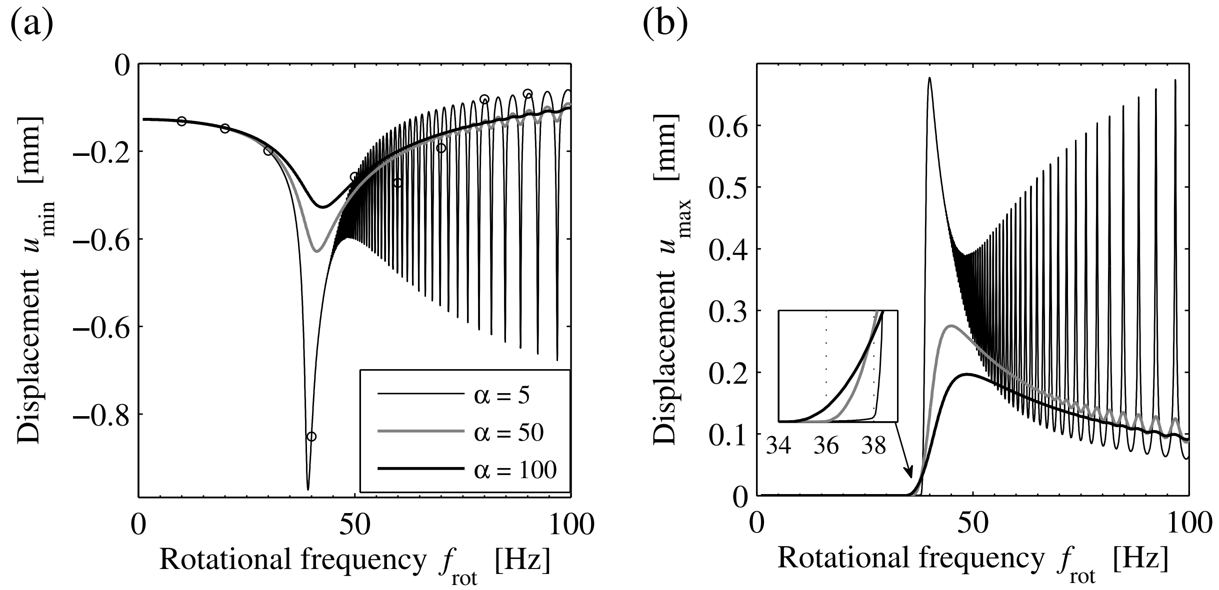

Figure 8: Minimum and maximum displacements of the cover in the rotational frequency range 1–100 Hz for three different values of the damping parameter α [Ns/m^2], (a) $u_{\min}$ and (b) $u_{\max}$. In (a), the balls mark results calculated with the centrifugal force included for $\alpha = 5$. The centrifugal force has a negligible effect on the system response, as discussed in Section 2.3. With small damping, $u_{\max}$ starts to increase from zero at a higher rotational frequency than with high damping, implying that the traveling wave phenomenon starts later with small damping due to higher wave phase velocities, see the insert in (b).

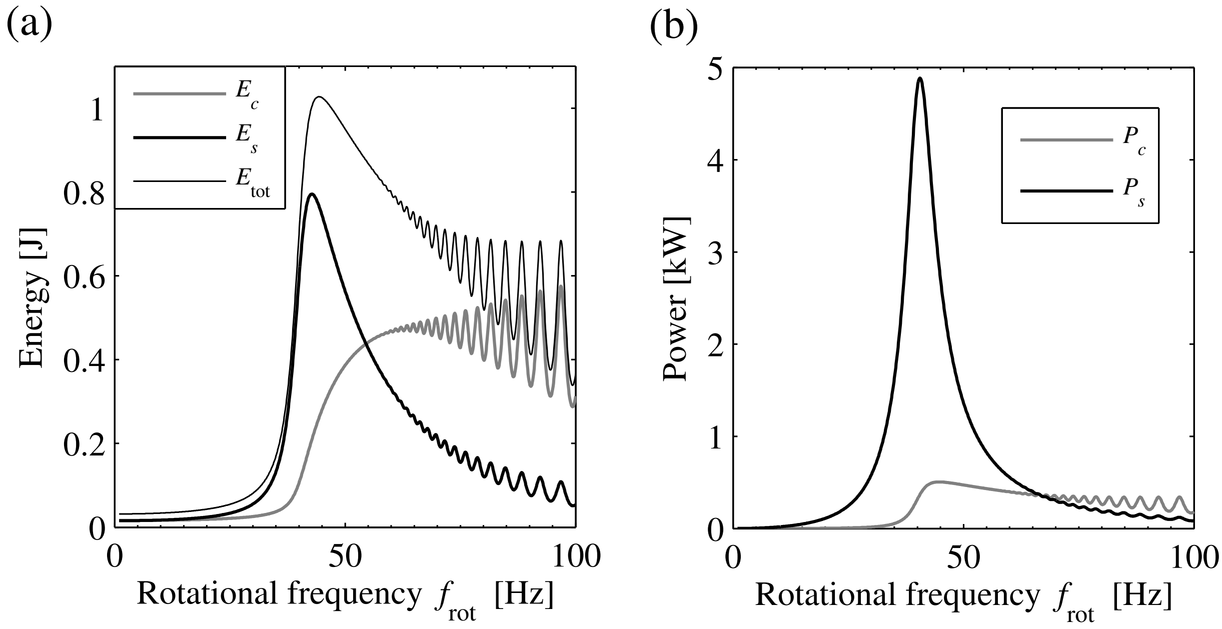

Figure 9: (a) Total, compressive and shear strain energies and (b) compressive and shear dissipation powers of the cylinder cover for $\alpha = 50$ Ns/m^2. When the wavelength of a traveling wave in the cylinder cover is short, that is, the curvature of the deformation is high, the shearing dominates both the deformation energy and power dissipation. At higher rotational frequencies, longer wavelengths become dominant, and compressive energy and power dissipation take over.

with the wavelength $\lambda_n = 2\pi R/n$ around the cylinder circumference. When the moving point load revolves around the cylinder, it excites the resonating mode n locally via the modal load (see Eqs. (4) and (5)). Furthermore, since the load always returns back to a point after one revolution and it is in phase with the oscillations generated at earlier visits, the cover vibration is reinforced. It is tempting to call this situation a reinforced resonance or a dual resonance. Note that this works also vice versa, that is, the traveling wave is weakened when the head and tail of the wave meet in antiphase at a rotational frequency which is between two consecutive resonant speeds. Similar resonances have also been found in the case of an elastic ring subjected to a moving load [19].

One way of evaluating the speed range within which the traveling wave phenomenon starts is to consider the ascent of the maximum displacement $u_{\max}$ from zero when the rotational frequency increases. This speed range is shown in detail in Fig. 8(b). It can be seen that with higher damping values, $u_{\max}$ starts to build up at lower rotational frequencies. This means that the critical speed range is lowered for increasing values of damping. The difference between the cases $\alpha = 5$ and $\alpha = 100$ Ns/m^2, for example, is about 3 Hz as can be seen in Fig. 8(b). A straightforward explanation from the wave propagation point of view is that additional damping drops the wave phase velocity, causing the traveling waves to appear earlier. It should be noted, however, that with high damping values the wave amplitudes rise slower and stay at relatively low values around the cylinder circumference. Therefore, the earlier appearance of the highly-damped traveling waves may be of minor practical importance in contrast to the case of low damping, where the wave amplitudes jump suddenly to high values around the whole cylinder circumference when the critical speed range is crossed. As mentioned earlier, Fig. 3(a) cannot alone say much about when the wave really starts to arise due to the wave attenuation caused by the damping.

Fig. 9(a) shows the total strain energy E_{tot} and its compressive and shear parts E_c and E_s, respectively, as a function of the rotational frequency of the moving load. Fig. 9(b) shows the compressive and shear dissipation powers P_c and P_s, respectively. The strain energies grow strongly when the traveling waves start to emerge. The shear part is dominant in the vicinity of the critical speed, that is, at shorter wavelengths,

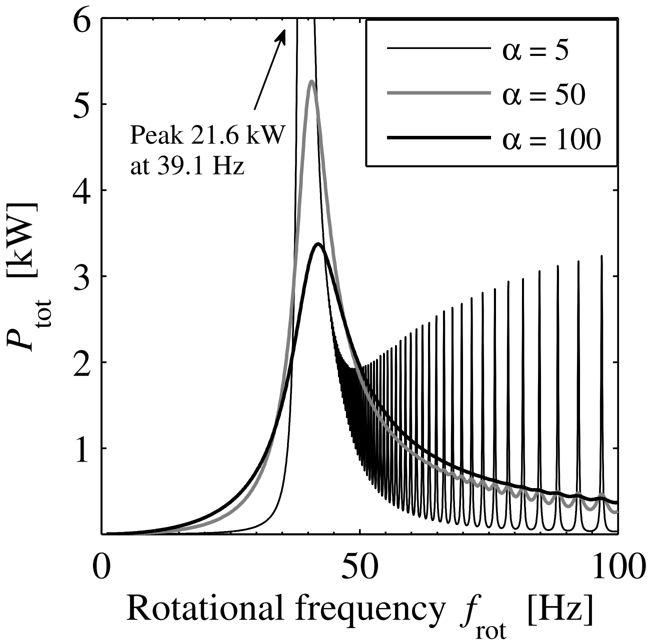

Figure 10: Total dissipation power for three different values of the damping parameter α [Ns/m^2]. High damping causes a remarkable increase in the total dissipation power at subcritical rotational frequencies, whereas low damping results in a high peak value and strong oscillations of the dissipation power in the supercritical area.

whereas at longer wavelengths the shearing of the cover reduces and the compressive strain dominates the deformation. In Fig. 9(b), it can be seen that the large dissipation power for incipient waving is almost completely due to shearing. However, at higher rotational frequencies the compressive damping becomes the dominant source of dissipation.

The dissipation power relates to the heat generation and rolling resistance of the cylinder cover. Excessive heating hastens the cover failure, and the power required to rotate a covered cylinder of an industrial machine increases in proportion to the dissipation power of the cylinder cover for increasing speeds. In practice, the traveling wave behavior is often observed only indirectly by monitoring the power levels. Fig. 10 presents the total dissipation power P_{tot} for three different values of the damping parameter α. With high damping, the dissipation power exhibits a significant increase already at subcritical rotational frequencies similarly to the rolling resistance of Qiu's 2D covered cylinder model [3]. The rise of the dissipation power is rather moderate within the critical speed range, and the dissipated peak power remains at a relatively low level. With low damping, the dissipation power remains low up to rotational frequencies quite close to the critical speed range. Then the power experiences a steep rise up to a very high peak value which is followed by an equally steep fall. Qiu studied the rolling resistance only at subcritical speeds, but the current model shows that, at supercritical speeds, the power oscillations start due to the dual resonances explained earlier. It can be seen that at the resonances the dissipated power attains high values, whereas between the resonances the power comes very close to zero. It can be concluded that high damping is a safe and predictable, although a power-consuming alternative, and can provide essential benefits in terms of the mitigation of the maximum vibratory response of a machine. Low damping, on the other hand, offers an opportunity to save power at both sub- and supercritical speeds, provided that the machine can be rapidly accelerated over the critical speed range and run accurately between the resonances in the supercritical area.

4. Conclusions

In this study, traveling waves in a cylinder cover subjected to a moving constant radial point load were investigated using a 1D Pasternak-type foundation model with Kelvin-Voigt damping. The model was validated by showing that the calculated natural frequencies and modes were in good concordance with those calculated from a more detailed 2D plane strain FE model. That is to say, the dynamic 2D plane strain problem can be essentially reduced to 1D. It was also shown that the centrifugal force has an inconsequential effect on the traveling waves in the cover of a cylinder rotating at realistic speeds; thus, the inverted approach with a moving load on a non-rotating cylinder was used for the study of the traveling waves. The main benefits from the 1D modeling approach are that the model is suitable to analytical study to a good extent, and in dynamic simulations the model can be faster by up to three orders of magnitude than the 2D FE model, depending on the nature of the simulation. The developed model also lends itself to further development through the use of complex elastic moduli to describe the cylinder cover as a frequency-dependent viscoelastic material, and may be used as a computationally cost-effective part of a larger model addressing also other dynamic aspects of a rolling contact machine.

It was shown analytically that in the undamped case the critical speed of the moving point load according to a resonance condition at which traveling waves first appear is also the minimum phase velocity of the waves in the cover. Wave dispersion causes the traveling waves to arise also at supercritical speeds. The phenomenon is analogous to the Rayleigh wave resonance in a 2D rolling contact case [4]. We want to emphasize that looking in detail at both of the interconnected aspects, vibration and wave propagation, may greatly facilitate in understanding the details and gaining a broader view on similar traveling wave phenomena.

The damped case was studied in detail computationally. With the addition of strain rate damping to the cover, the critical speed dropped along with the wave speeds and became blurred. Increasing damping caused the waves to emerge at even lower speeds. However, strong damping attenuates the waves efficiently around the cylinder circumference. With low damping, in particular, reinforced resonances could be observed at supercritical speeds when the head and tail of a traveling wave joined smoothly. In such a situation, one resonating mode dominates the cover response, which can be also viewed as an aide to wave propagation. High damping, although helpful in the mitigation of vibrations, caused considerable power dissipation already at subcritical speeds. With low damping, power can be saved, but the system exhibits a powerful shock-like response if the critical speed is approached.

Acknowledgment

The financial support from the Ministry of Education and Culture of Finland through the Graduate School of Engineering Mechanics is gratefully acknowledged.

References

[1] A. Sueoka, T. Ryu, T. Kondou, Y. Tsuda, K. Katayama, K. Takasaki, M. Yamaguchi, H. Hirooka, Polygonal deformation of roll-covering rubber, *JSME International Journal, Series C*, 39 (1) (1996) 1-10.

[2] A.T. Karttunen, R. von Hertzen, Polymer cover induced self-excited vibrations of nipped rolls, *Journal of Sound and Vibration*, 330 (16) (2011) 3959-3972.

[3] X. Qiu, Full two-dimensional model for rolling resistance. II: Viscoelastic cylinders on rigid ground, *Journal of Engineering Mechanics*, 135 (1) (2009) 20-30.

[4] A.T. Karttunen, R. von Hertzen, A numerical study of traveling waves in a viscoelastic cylinder cover under rolling contact, *International Journal of Mechanical Sciences*, 66 (2013) 180-191.

[5] R.V. Goldstein, Rayleigh waves and resonance phenomena in elastic bodies, *Journal of Applied Mathematics and Mechanics*, 29 (3) (1965) 608-619.

[6] H.A. Dieterman, A.V. Metrikine, The equivalent stiffness of a half-space interacting with a beam. Critical velocities of a moving load along the beam, *European Journal of Mechanics – A/Solids*, 15 (1) (1996) 67-90.

[7] J.T. Oden, T.L. Lin, The general rolling-contact problem for finite deformations of a viscoelastic cylinder, *Computer Methods in Applied Mechanics and Engineering*, 57 (3) (1986) 297-367.

[8] J. Padovan, Finite-element analysis of steady and transiently rolling nonlinear viscoelastic structure, 1. Theory. *Computers & Structures*, 27 (2) (1987) 249-257.

[9] Y. Waki, B.R. Mace, M.J. Brennan, Free and forced vibrations of a tyre using a wave/finite element approach, *Journal of Sound and Vibration*, 323 (3-5) (2009) 737-756.
[10] G.-P. Zehil, H.P. Gavin, Three-dimensional boundary element formulation of an incompressible viscoelastic layer of finite thickness applied to the rolling resistance of a rigid sphere, *International Journal of Solids and Structures*, 50 (6) (2013) 833-842.
[11] S.C. Huang, W. Soedel, Response of rotating rings to harmonic and periodic loading and comparison with the inverted problem, *Journal of Sound and Vibration*, 118 (2) (1987) 253-270.
[12] A. Chatterjee, J.P. Cusumano, J.D. Zolock, On contact-induced standing waves in rotating tyres: Experiment and theory, *Journal of Sound and Vibration*, 227 (5) (1999) 1049-1081.
[13] A.D. Kerr, Elastic and viscoelastic foundation models, *Journal of Applied Mechanics*, 31 (3) (1964) 491-500.
[14] W. Soedel, On the dynamic response of rolling tires according to thin shell approximations, *Journal of Sound and Vibration*, 41 (2) (1975) 233-246.
[15] J. Padovan, Traveling waves vibrations and buckling of rotating anisotropic shells of revolution by finite elements, *International Journal of Solids and Structures*, 11 (12) (1975) 1367-1380.
[16] J. Padovan, On viscoelasticity and standing waves in tires, *Tire Science and Technology*, 4 (4) (1976) 233-246.
[17] G.R. Cowper, Shear coefficient in Timoshenko's beam theory, *Journal of Applied Mechanics*, 33 (2) (1966) 335-340.
[18] K.F. Graff, *Wave Motion in Elastic Solids*, Clarendon press, 1975.
[19] A.V. Metrikine, M.V. Tochilin, Steady-state vibrations of an elastic ring under a moving load, *Journal of Sound and Vibration*, 232 (3) (2000) 511-524.